J Mater Sci: Mater Electron (2017) 28:8437–8445
DOI 10.1007/s10854-017-6562-x

CrossMark

Machining damage of monocrystalline silicon by specific crystallographic plane cutting of wire electrical discharge machining

Mengxing Ge[1] · Zhidong Liu[1] · Haoran Chen[1] · Lida Shen[1] · Mingbo Qiu[1] · Zongjun Tian[1]

Received: 28 December 2016 / Accepted: 7 February 2017 / Published online: 21 February 2017
© Springer Science+Business Media New York 2017

Abstract The machining damage on the certain crystal face of single crystal silicon, the manufacture of which are under diverse parameters of wire electrical discharge machining (WEDM), is tested by means of the micro-observation and X-ray diffraction rocking curve method. In the process of monocrystalline silicon machined by WEDM, when the pulse width is small, the basic methods of material removal are melting and gasification, which are also called normal removal methods. When the pulse width increases to a certain degree beyond the normal removal, thermal spalling removal also occurs, which is considered a compound removal method. The depth of machining damage is difficult to control. The structure of machining damage under two conditions is divided into normal removal and compound removal in this study. To make the depth of machining damage easy to control, compound removal should be avoided when processing the single crystal silicon by certain crystal face cutting of WEDM. Such an approach can provide the premise and guarantee for the subsequent processing of single crystal silicon with certain crystal face in the future.

Keywords Wire electrical discharge machining · Specific crystallographic plane · Machining damage · Monocrystalline silicon · X-ray diffraction rocking curve method

✉ Zhidong Liu
liutim@nuaa.edu.cn

[1] College of Mechanical and Electrical Engineering, Nanjing University of Aeronautics and Astronautics, Yu Dao Street, Nanjing 210016, China

1 Introduction

Silicon is an important and widely used semiconductor crystal material and is recognized as the foundation of modern information society [1]. Monocrystalline silicon is a primary material in integrated circuits because of its good heat and radiation resistance. This material is extensively applied as a common material to produce diffraction crystals in condensed matter physics, high-energy physics, materials chemistry, and other fields. Monocrystalline silicon with a specific crystallographic plane is used to manufacture the core parts of neutron scattering spectrometers [2], X-ray diffraction spectrometers [3], nuclear resonance and lithography apparatuses [4], and other equipment. To produce electrical components or the diffraction crystals in optics, the surface of monocrystalline silicon must be bright, clean, without any damage, highly smooth, and with a precise crystal orientation [5, 6]. WEDM is extensively applied in the certain crystal face cutting of single crystal silicon, which results in the absence of macroscopical cutting force, large machining size, high cutting precision, and low loss. However, the processing properties of WEDM often cause machining damage on the processing surface, called damage layer which includes lattice distortion, residual stress, cracks, small holes, discharge craters, and other machining damages [7]. Given the special physical properties of monocrystalline silicon, its damage layer is different from that of ordinary metals.

Many studies have focused on the machining damage of monocrystalline silicon by WEDM [8–10]. However, the research on the influence of different removal methods on silicon crystal, structure characteristics, and depth of machining damage is not thorough. Research methods are mainly microscopic observation. This paper adopts the X-ray diffraction rocking curve method combined with the

microscopic observation method to study the damage structure of a single crystal silicon machined by certain crystal face cutting of WEDM under different pulse widths. This approach provides basic protection for the subsequent processing of the surface of the monocrystalline silicon and for the final realization of high precision. As a result, no processing damage will occur on the surface of the single crystal silicon with certain crystal face.

2 Experiment system and measurement

The silicon wafers were processed by HF400D WEDM machine-tool which has a large taper-cutting function. Wire-feeding system of this machine is shown in Fig. 1. The processing parameters and conditions of 5 groups of silicon wafers are listed in Table 1.

The wafer surface is detected by an YX-2 crystal orientation inspection apparatus (Fig. 2) and a screw micrometer. The back rocking curves are drawn according to the experimental data. The measured surface of silicon wafer is observed by an S-3400N scanning electron microscope (SEM). The damage layer thickness and structure are then calculated through data processing and image analysis. During the experiment, quantitative corrosion device (Fig. 3) is used to etch silicon wafers. It uses a quantitative corrosion device for the corrosion on the silicon wafer surface to make the corrosion thickness of the silicon controllable. An electrical control box controls the motor to drive the screw movement; thus, the fixed corrosion-resistant wafer holder clamp can move up and down. The single-chip microcomputer in the control box controls the corrosion time and the speed of silicon wafer when lifting up and down. An acid corrosion solution with isotropic characteristics is used for the corrosion of silicon wafers [11] (the specific parameters are shown in Table 2).

The process of the experiment is summarized below. Silicon wafers (pulse width: 40 μs) were used in the

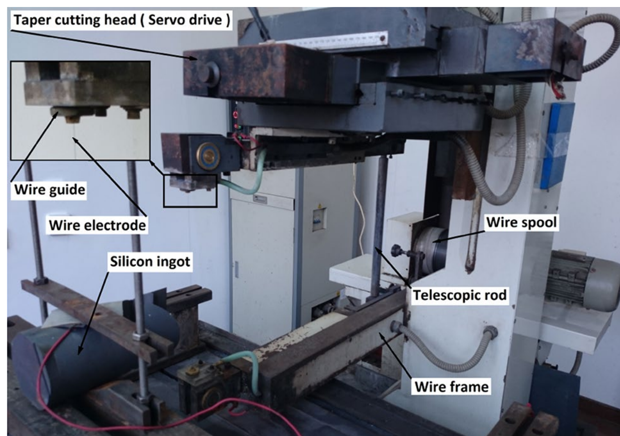

Fig. 1 Wire-feeding system of HF400D WEDM machine-tool

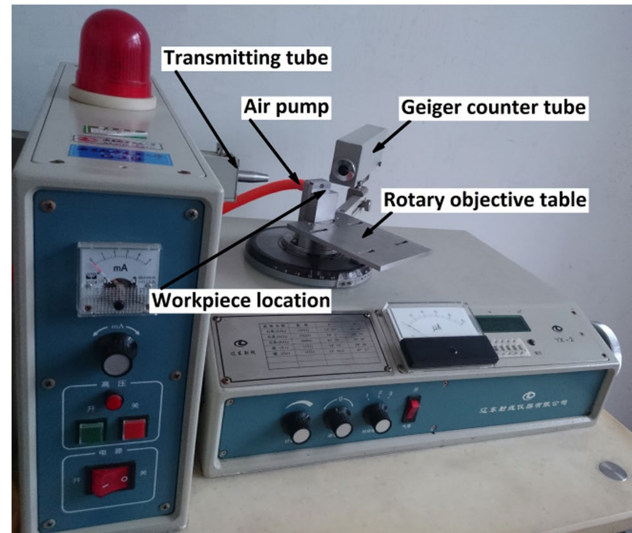

Fig. 2 YX-2 crystal orientation inspection apparatus

Table 1 Processing parameters and conditions of 5 groups of silicon wafers

Parameter	Unit	Range and levels				
No.		1	2	3	4	5
T_{on}	μs	5	10	20	40	80
Open circuit voltage	V	140				
Peak current	A	6				
Wire speeds	m/s	7.2				
Duty ratio (T_{on}:T_{off})	–	1:8				
Crystal orientation	–	(110)				
Working liquid	–	Water-based compound working liquid				
Work piece material	–	P-type single crystal silicon (1.2 Ω·cm)				
Tool-electrode	–	Electrode wire (molybdenum, Φ0.18 mm)				
Polarity	–	Workpiece (+)				

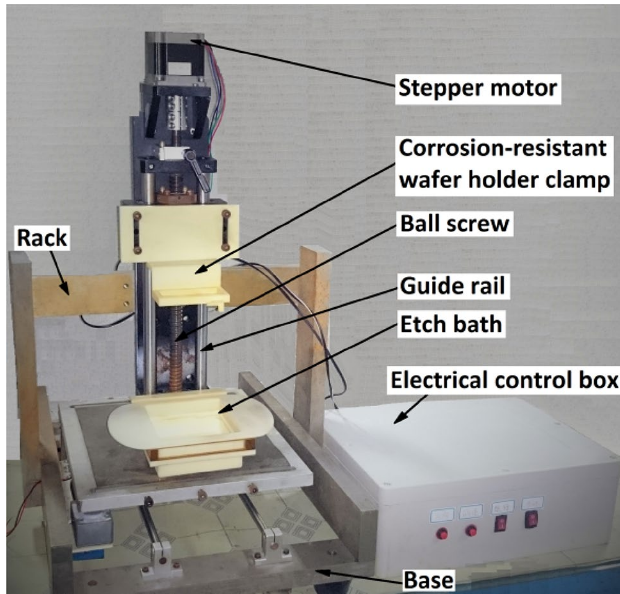

Fig. 3 Quantitative corrosion device

Table 2 Corrosion parameters

Parameter	Values
HF (40–42%)	10 ml
HNO_3 (65%)	25 ml
Corrosion time	0.2 min
Temperature	20–25 °C

experiment and called wafer 1 as an example (other wafers are tested in the same manner).

1. Measure initial thickness d (The distance between top and bottom surface [2 crystal face(110)] of silicon wafer) of wafer 1.
2. Use the YX-2 crystal orientation inspection apparatus to test one surface (110 surface) of wafer 1. Record the values of the diffraction relative intensity and corresponding angle. Plot the rocking curves diagram and obtain value of the full width at the half maximum (FWHM) [12, 13].
3. Take a picture of the measured surface (110 surface) with SEM.
4. Place the measured surface of wafer 1 to a chemical solution and corrosion for 12 s. Take out wafer 1. Measure thickness d of wafer 1 after it was washed and dried.
5. Carry out step 2 and start looping (5-2-3-4-5). Compare the values of FWHM after each test and stop looping until FWHM remains constant.
6. Draw the $d - \Delta\theta$ relationship curve diagram of wafer 1.

The details of the experiment process are shown in Fig. 4. Only the measured face of the silicon wafer was submerged in chemical solution. Three uniform distribution regions (A, B, and C) on the measured face of the wafer must be detected during the process. The diagrams of the rocking curves and the $d - \Delta\theta$ relationship curves are drawn based on the average values of the A, B, and C regions. Thus, errors of experiment arising due to uneven corrosions can be reduced. The depth error of the damage layer is mainly from the minimum division value of the screw micrometer (0.001 mm) and the YX-2 crystal orientation inspection apparatus (0.5′) [13].

X-ray diffraction rocking curve method, on the base of Bragg's law (Fig. 5), was adopted to test the processed silicon wafer's damage layer. According to the Bragg diffraction theorem, when X-ray irradiates on the crystal surface, Bragg angle θ will correspond to an alteration of Δθ if the interplanar diffracted area (spacing d) changes Δd [12]. If a crystal exhibits cracks, small holes, dislocation, or other surface damage, the diffractive angle of X-ray will alter within limits, which increases the values of FWHM; when machining damage is removed, the value of FWHM tends to be constant [13]. Thus, the machining damage can be removed layer by layer through quantitative corrosion,

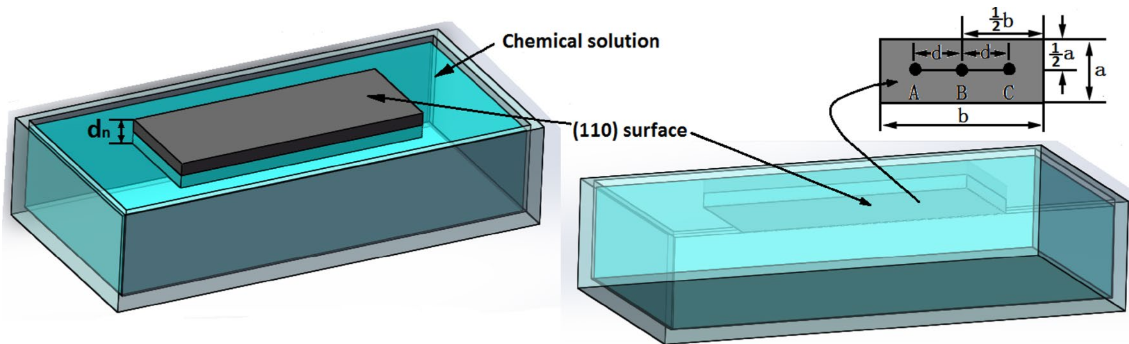

Fig. 4 Sketch of detection details

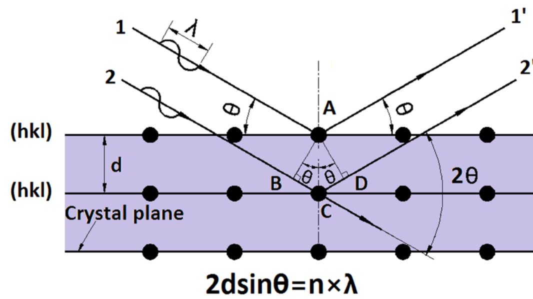

Fig. 5 Bragg diffraction schematic diagram

and after each corrosion the YX-2-type crystal instrument and S-3400N SEM can be used to test the (110) crystal plan of silicon wafers. According to the changes in values of FWHM and SEM graphs, the depth and corresponding structure of silicon-machining damage can be calculated.

3 Results and analysis

3.1 3.1 Removal form and damage mode

Taking silicon wafer 1 [(110) crystal plane, 40 µs pulse width] as example, the structure of machining damage on monocrystalline silicon by WEDM is analyzed layer by layer through SEM observation. After each corrosion (the removal thickness and corresponding figure number of corrosion surface are shown in Table 3), we observe the etched surface of silicon wafer using the S-3400N SEM. The micrograph is shown in Fig. 6a–j.

By the thickness values (d) of single crystal silicon removed through corrosion of silicon wafer 1 and their corresponding FWHM values (Δθ), a curve of $d - \Delta\theta$ relationship (Fig. 7) could be produced. Given that the damage layer contains holes, cracks, dislocation, and many other crystal imperfection, structure changes are relative to the silicon substrate. And under the damage layer the silicon substrate appear. The inflection point in Fig. 7 signify a value of FWHM and its corresponding thickness of removed, from which FWHM value remains unchanged (corrosion occurs on substrate), and the corresponding thickness is the thickness of damage layer [13].The correspondence between the $d - \Delta\theta$ relation curve and the damage layer structure is thus as follows: AD corresponds to the damage layer region; DE corresponds to the substrate region; the damage layer region can be divided into three parts, which corresponds to AB, BC, and CD. AB corresponds to Fig. 6a, b. This section is full of cracks and holes. As for the early corrosion, the pits in the figure are discharge craters. BC corresponds to Fig. 6c, d. The distribution density of the holes and craters gradually reduces to zero, and cracks are decreased. CD corresponds to Fig. 6e–i. Cracks continue to reduce, and the lattice distortion and other structure damage are also gradually removed. DE corresponds to Fig. 6j. This section has a smooth surface without damage, which has already arrived in the substrate.

Figure 7 illustrates that the AB, BC, and CD segments in the $d - \Delta\theta$ relation curve have a certain slope. The slope section presents the FWHM value changes, which correspond to each removed damage layer thickness. The decrease rate of the FWHM value of AB in Fig. 7 is the fastest; the decrease rates of BC and CD sections are reduced successively; and the FWHM value of DE remains unchanged.

WEDM produces discharge craters and micro-cracks on the machined surface of silicon slice and disrupts the arrangement of silicon atoms near or within a certain depth range under the machined surface, that can vary the lattice parameter (a_0). This variation decreases gradually with the deepening of the silicon wafer. Moreover, holes, cracks, dislocation, and many other crystal imperfection alter diffractive angle of X-ray within limits, which also make the FWHM value of X-ray rocking curve increased [12]. With growing thickness of removed single crystal silicon, the inspection surface of silicon wafer becomes close to silicon substrate, crystal imperfection taper off, array of silicon atoms get orderly; and then the FWHM value gradual decline [13], and the decrease rate of the FWHM value reduces gradually. When corrosion occurs on substrate where no crystal imperfection exist and atoms are arranged orderly, the diffractive angle of X-ray remains the same, and so FWHM value remains unchanged.

According to the experimental data, we fit the $d - \Delta\theta$ relationship summarized graph (see Fig. 8) of silicon wafers with different pulse widths of 5, 10, 20, 40, and 80 µs (other processing parameters are the same).

Figure 8 shows the single crystal silicon machined by certain crystal face cutting of WEDM, with different pulse widths of 5, 10, 20, 40, and 80 µs (other processing parameters are the same); its initial FWHM value increases in turn. After corrosion on the substrate, the FWHM values

Table 3 Removal thickness and corresponding figure number of corrosion surface

Number of corrosion	1	2	3	4	5	6	7	8	9	10
Removal thickness of each corrosion (µm)	12	11	11	12	13	12	13	12	12	11
Figure number of surface after corrosion	a	b	c	d	e	f	g	h	i	j

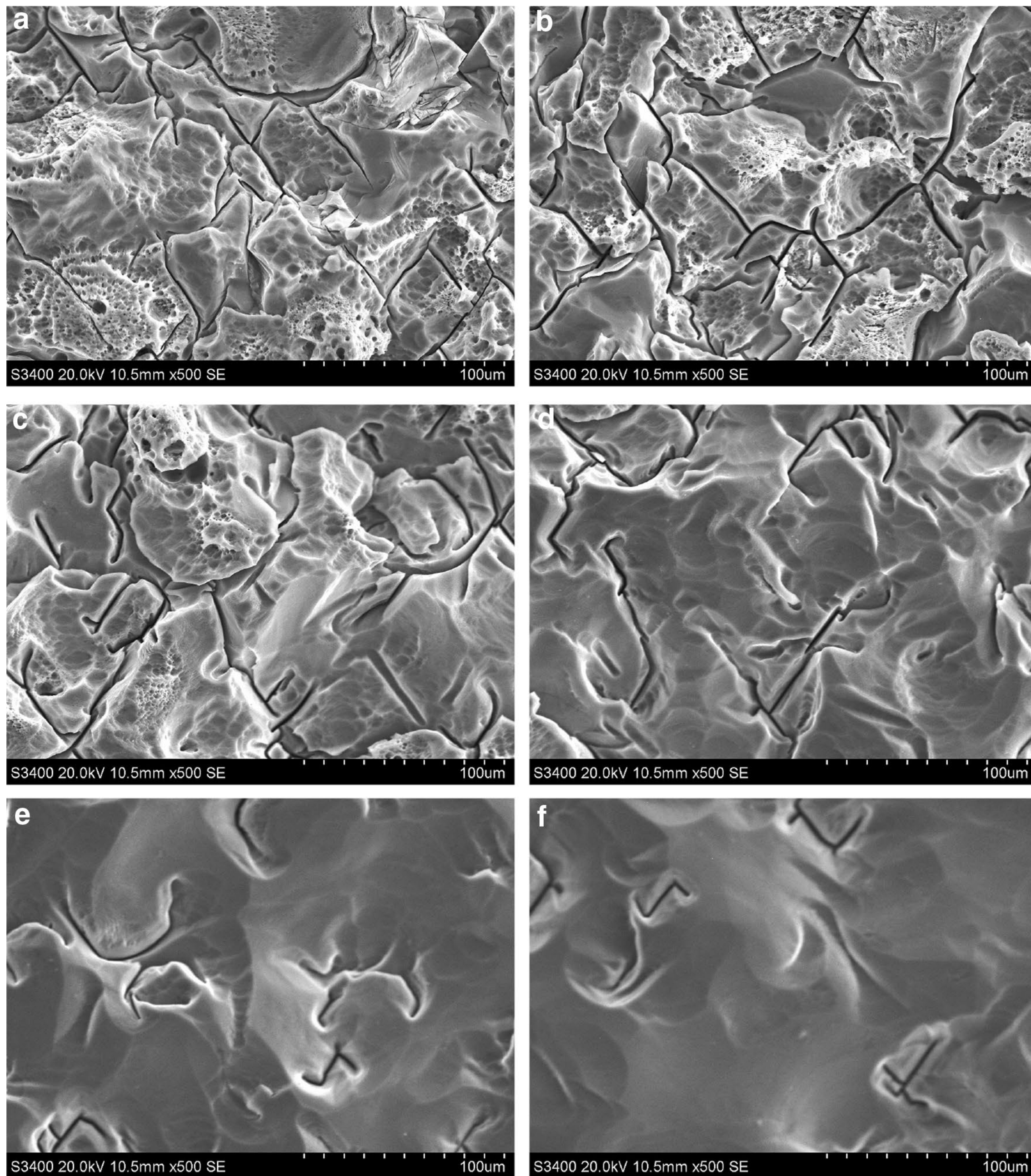

Fig. 6 Damage layer microstructure graphs after each corrosion

remain stable at 3.5′. Damage layer thickness increases with an increase in pulse width; both are positively correlated. For the silicon with pulse widths of 5, 10, 20, and 40 µs, after the corrosion with a uniform test point distribution, the FWHM value decreases with an increase in corrosion removal thickness. By contrast, when the pulse width is 80 µs, the detection point distribution of silicon wafer after each corrosion is nonuniform, and the FWHM value is detected at 3.5′ before corrosion on the substrate (as shown in Fig. 8; the triangle points in circle). 3.5′ is the FWHM value of the substrate, which shows that before etching to silicon substrate, the X-ray diffractometer has detected the testing point for the base material. Therefore, thermal spalling happens on this point in the processing [14], namely, crystal silicon cleavage cracks along the key with a weak binding force; the formed surface is the same as the cleavage plane, and although the spalling face is the same as the cleavage plane, some point of which has reached the substrate. Nevertheless, the spalling face is still a kind of injury for the surface of the single crystal silicon

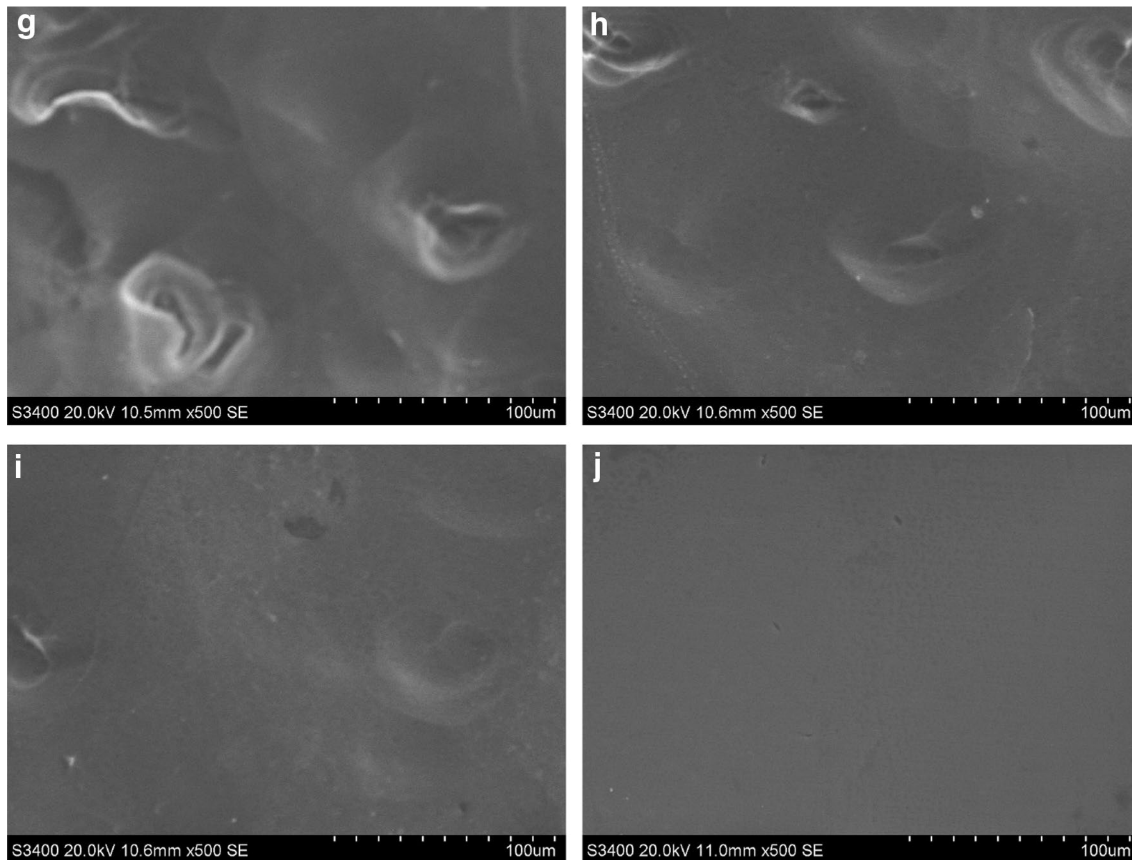

Fig. 6 (continued)

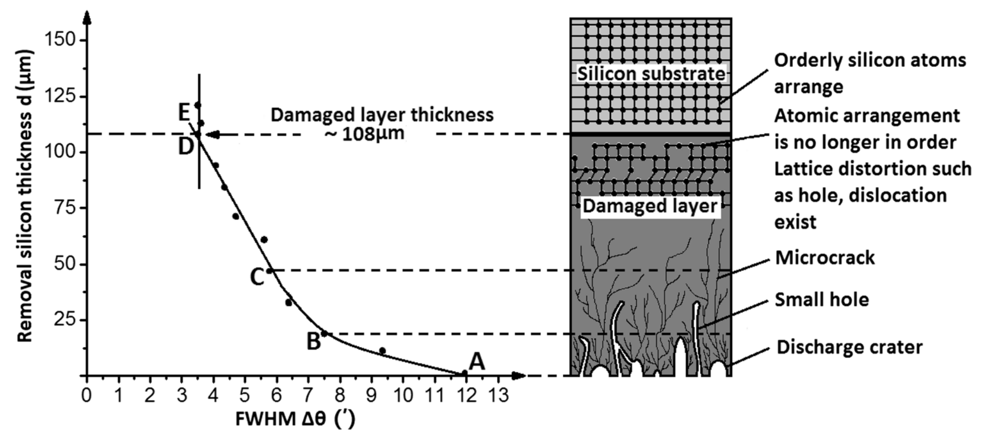

Fig. 7 d – Δθ relationship curve and the corresponding sketch of damage layer removal

crystal machined by certain crystal face cutting of WEDM, and the depth of which is unknown.

For the silicon with a pulse width of 80 μs in removing thickness of 0–50 microns, 50–100 microns, and 100–150 microns, the point with FWHM value at 3.5′ appears in all these three ranges (as shown in Fig. 8; the triangle points in circle). Thus, silicon wafer spalling exists within the three ranges. After the pulse width increases to a certain degree, spalling is irregular and uncontrollable, which causes an uncontrolled machining damage depth of silicon wafer. This characteristic is also the difference between monocrystalline silicon and metal, that is, spalling will not occur after the WEDM for metal. The spalling phenomenon (Fig. 9) is caused by thermal stress spalling removal. When the other processing parameters are the same, a great pulse width leads to a long duration of the discharge quantity of

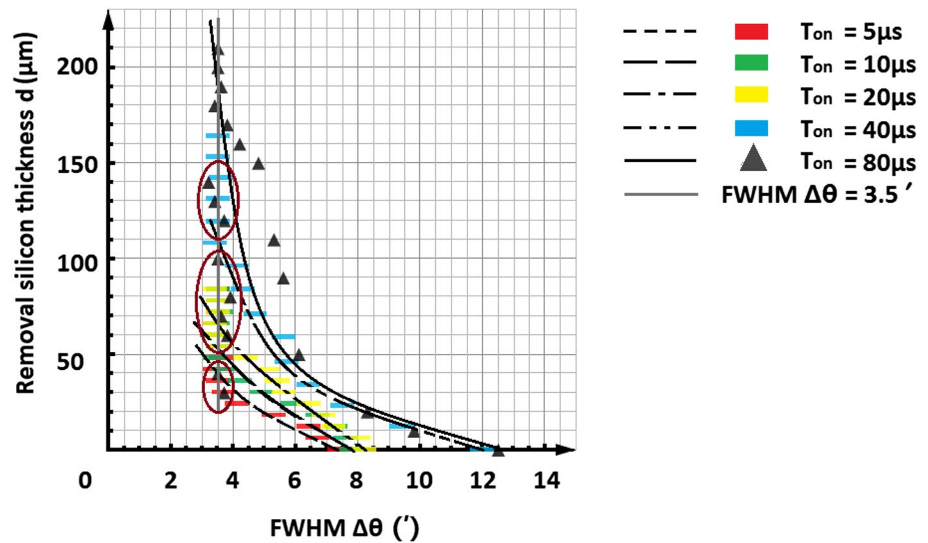

Fig. 8 d – Δθ relationship summarized graph

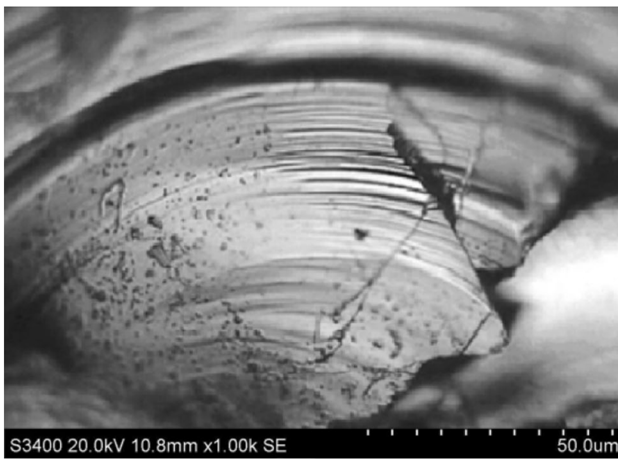

Fig. 9 Spalling phenomenon

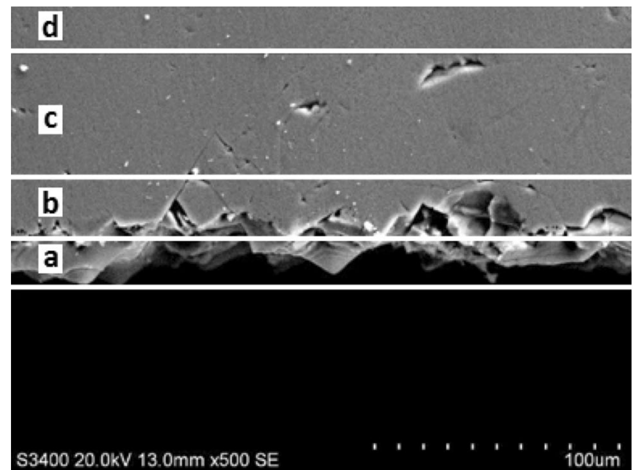

Fig. 10 SEM graph of monocrystalline silicon machined by WEDM

heat, which is not easy to spread. Considerable heat is then concentrated in a small area, thereby making the region form a large temperature gradient that causes the thermal stress of the internal of the material sharply increase. When the thermal stress increases to a certain extent, lattice dislocation and slip happen. Thermal stress spalling removal occurs because of significant explosion removal force as well as the hard brittle characteristics of monocrystalline silicon, partial dislocation, slip cleavage along the key with a weak binding force under thermal stress, and plasma channel material inflation pressure, which further develops into micro cracks that spread on the surface.

Figure 8 presents that the manufacture of monocrystalline silicon machined by WEDM in which the way of silicon removal is divided into two types. With silicon machined with pulse widths of 5, 10, 20, and 40 μs, the basic ways of material removal are melting and gasification [14], which are defined as normal removal. With silicon machined with a pulse width of 80 μs, beyond the normal removal, thermal stress spalling removal also happens, which is defined as compound removal. Given that the thermal stress spalling removal is uncontrolled and damages deeply the surface of silicon wafer, it can take the way of reducing pulse width to avoid compound removal, thus achieving the purpose of controllable damage depth and reduced machining damage thickness.

3.2 Structure of machining damage

The damage layer microstructure of a monocrystalline silicon machined by WEDM can be subdivided into four parts, namely, a, b, and c areas that constitute the damage layer and d area for substrate (see Fig. 10). The a, b, c, and d

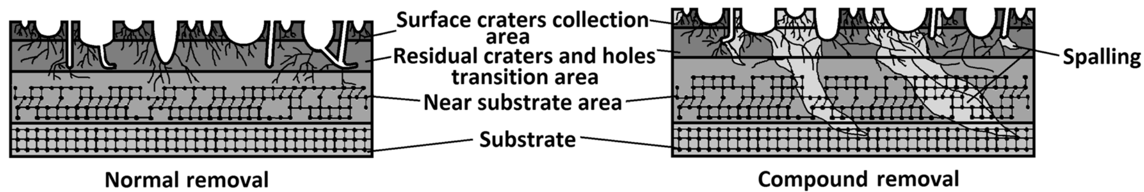

Fig. 11 Damage structure schematic

areas in Fig. 10 correspond to the AB, BC, CD, and DE of the $d-\Delta\theta$ relation curve, respectively.

When the pulse width is small, the basic ways of material removal are melting and gasification, which are the process of normal removal. On regions a, b, and c, the depths of discharge crates, cracks, and holes are small, and the spalling phenomenon caused by thermal stress and explosion power rarely happens. In the normal removal process, the machining damage structure of monocrystalline silicon by WEDM is the structure of damage layer, which can be divided into (from the surface to the center) surface crater collection area, residual crater and hole transition area, and near substrate area. The schematic of the damage structure is shown in Fig. 11.

When the pulse width increases to a certain degree, beyond the normal removal, thermal spalling removal also happens. This type of material removal is a compound removal. The depths of discharge crates, cracks, and small holes on areas a, b, and c are large, and a significant cleavage plane caused by the spalling phenomenon appears in a, b, c, and d areas. The cleavage plane can reach the substrate, and the depth of spalling is uncontrollable. Consequently, the depth of machining damage is not easy to control and cannot be polished accurately. In case of compound removal, the machining damage structure of monocrystalline silicon by WEDM consists of damage layer and the spalling damage, and the division of the damage layer is the same as that in normal removal. A spalling damage with an uncontrolled depth appears in the damage layer and substrate area.

4 Conclusion

1. Material removal in the process of monocrystalline silicon machined by WEDM can be divided into two types: when the pulse width is small, the basic ways of material removal are melting and gasification, which are defined as normal removal method; when the pulse width increases to a certain degree beyond the normal removal, thermal spalling removal also occurs, which is defined as compound removal method.
2. During the process of compound removal, a significant cleavage plane caused by the spalling phenomenon appears. The cleavage plane can reach the substrate, and the depth of machining damage is uncontrollable and cannot be polished accurately. Therefore, pulse width should be reduced to avoid compound removal when processing the single crystal silicon by certain crystal face cutting of WEDM.

Acknowledgements This paper is supported by Funding of Jiangsu Innovation Program for Graduate Education (the Fundamental Research Funds for the Central Universities) (Grant No. KYLX15_0291) and the National Natural Science Foundation of China (Grant Nos. 51575271, 11275274, U1532106). We would like to thank all of people who contributed to this project.

References

1. M.A. Chun, Development trend of semiconducting silicon materials of the world. Shanghai Nonferrous Met. **26**(3), 145–148 (2005)
2. M.W. Johnson, S. Manolopoulos, N.J. Rhodes et al., Silicon APS detectors for neutron scattering. Nucl. Instrum. Methods Phys. Res. Sect. A **501**, 72–79 (2003)
3. J. Słowik, A. Zięba, Silicon strip detector applied to X-ray diffractometer: angular resolution and counting rate. Nucl. Instrum. Methods Phys. Res. **551**(1), 73–77 (2005)
4. Y. Wang, J. Kang, Development and challenges of lithography for ULSI. Chin. J. Semicond **3**, 225–237 (2002)
5. Q. Zhang, H. Zhou, D. Li, Indention microcrack formation and propagation in single crystalline silicon at room temperature. J. Chin. Electron Microsc. Soc **21**(1), 56–58 (2002)
6. U. Bismayer, E. Brinksmeier, B. Guttler et al., Measurement of subsurface damage in silicon Wafers. Precis. Eng **16**(2), 139–143 (1994)
7. Z. Liu, W. Wang, M. Qiu, Basic research on compound EDM and ECM cutting with texturing on solar wafer. Acta Energiae Solaris Sinica **30**(5), 619–623 (2009)
8. G. Kühn, H. F. Hadamovsky (Hrsg.). Werkstoffe der Halbleitertechnik. 2. Aufl. Deutscher Verlag für Grundstoffindustrie Leipzig 1990, 360 Seiten mit zahlreichen Abbildungen und Tabellen, Literatur-und Sachwortverzeichnis, Preis 68, — DM, ISBN 3–342–00315–4. Cryst. Res. Technol. **27**(1), 58–58 (1992)
9. L. Zhang, I. Zarudi, Towards a deeper understanding of plastic deformation in mono-crystalline silicon. Int. J. Mech. Sci **43**(9), 1985–1996 (2001)
10. G.G. Dongre, C. Vesivkar, R. Singh, S.S. Joshi, Modeling of silicon ingot slicing process by wire-electrical discharge machining. Proc. IMechE Part B J. Eng. Manuf **227**(11), 1664–1678 (2013)

11. D. Chen, Chemical etching of silicon (review). Spec. Electr **3**, 35–37 (1983)
12. Z. Zhao, *Cutting Semiconductor Crystal with Specific Orientation*. (Science Press, Beijing, 1979)
13. M Ge, Z Liu, L Shen et al., Thickness measurement of deterioration layer of monocrystalline silicon by specific crystallographic plane cutting of wire electrical discharge machining. J. Mater. Sci. Mater. Electron. 27(9), 9107–9114, (2016). doi:10.1007/s10854-016-4945-z
14. Z. Liu, L. Gao, M. Qiu, Z. Tian, W. Wang, Study on damage mechanism of monocrystalline silicon cut by WEDM. Acta Aeronauticaet Astronautica Sinica **1**, 156–162 (2012)